RESEARCH ARTICLE

Biogeochemical gradients and microbial communities in Winogradsky columns established with polluted wetland sediments

Izabella Babcsányi, Fatima Meite and Gwenaël Imfeld*

Laboratory of Hydrology and Geochemistry of Strasbourg (LHyGeS), University of Strasbourg/EOST, CNRS, 1 rue Blessig, 67084 Strasbourg Cedex, France

*Corresponding author: Laboratoire d'Hydrologie et de Géochimie de Strasbourg (LHyGeS), Université de Strasbourg/EOST, CNRS, 1 rue Blessig, 67084 Strasbourg Cedex, France; Tel: +333-6885-0474; Fax: +333-8824-8284; E-mail: imfeld@unistra.fr
One sentence summary: Microbial communities and heavy metal biogeochemical analyses in Winogradsky columns revealed that microbial communities are diverse and determined by geochemical stratification.
Editor: Alfons Stams

ABSTRACT

A Winogradsky column is a miniature ecosystem established with enriched sediments that can be used to study the relationship between biogeochemical gradients, microbial diversity and pollutant transformation. Biogeochemical processes and microbial communities changed with time and depth in Winogradsky columns incubated with heavy-metal-polluted wetland sediments for 520 days. 16S rRNA surveys were complemented by geochemical analyses, including heavy metal proportioning, to evaluate gradients in the mostly anoxic columns. Oxygen was depleted below the water–sediment interface (WSI), while NH_4^+, Fe^{2+}, S^{2-} and acetate increased by one order of magnitude at the bottom. Microbial niche differentiation occurred mainly by depth and from the light-exposed surface to the interior of the columns. Chemical gradients resulting from nutrient uptake by algae, and from iron and sulphate reduction mainly drove diversification. Heavy-metal proportioning did not significantly influence microbial diversity as Cu and Zn were immobilised at all depths. Proteobacteria were abundant in the top water and the WSI layers, whereas Firmicutes and Bacteroida dominated down-core. Together with low diversity and richness of communities at the WSI and column bottom, changes in the bacterial community coincided with algal-derived carbon sources and cellulose fermentation, respectively. We expect this study to be the starting point for the use Winogradsky columns to study microbial and geochemical dynamics in polluted sediments.

Keywords: heavy metal pollution; microbial indicators; biogeochemical cycles; wetland

INTRODUCTION

A Winogradsky column is a miniature ecosystem that can be used as a model system to study microbial communities involved in biogeochemical cycles and the transformation of pollutants. Over space and time, numerous, uncontrollable physicochemical factors have an impact on microbial communi-ties involved in the transformation of pollutants in natural sediments, which hampers study of their development (Lüdemann, Arth and Liesack 2000; Van der Gucht *et al.* 2007). By contrast, the Winogradsky sediment column expands the volume of natural processes, enabling microbial communities to grow in stratified ecosystems created by chemical gradients (Winogradski 1888;

Dworkin 2012). As Winogradsky columns can be replicated and maintained under controlled conditions, they offer an opportunity to study how microbial communities and biogeochemical processes stratify and affect pollutant transformation in sediments.

In aquatic ecosystems, heavy metals are usually bound to particles and settle in bottom sediments, where they accumulate (Machado *et al.* 2016). Steep physicochemical gradients formed locally over time in sediments have an impact on microbial communities and biogeochemical processes, thereby controlling pollutant transformation and transport to other compartments of the aquatic system (Borch *et al.* 2010; Pedersen, Smets and Dechesne 2015). Heavy metals precipitate under reducing conditions as metal-sulphide species or mixed heavy metal–iron sulphides (Morse and Luther 1999; Machado *et al.* 2016). Depending on the prevailing redox conditions, heavy metals can be released in the form of colloidal metal and sulphide particles (Weber *et al.* 2009) during the reductive dissolution of metal-sorbing oxide-hydroxides or oxidation of reduced metal species (Gounou *et al.* 2010; Simpson *et al.* 2012). However, little is known about the interaction between biogeochemical processes and microbial diversity along redox gradients established in heavy metal-polluted sediments.

In the Winogradsky column, photosynthetically active organisms at the column surface use light, and nutrient cycling is sustained as the structured microbial ecosystem develops. Redox gradients from the top to bottom and surface to interior of the column are established as algae produce oxygen in the overlying water and aerobic microorganisms gradually consume oxygen downwards in the column. In the anoxic sediments down-core, sulphate-reducing microorganisms produce H_2S that diffuses upwards in the column and create a sulphide gradient. Winogradsky columns have been used previously to study photosynthetic sulphur and non-sulphur bacteria (Martinez-Alonso *et al.* 2006; Loss *et al.* 2013), spatial changes in the bacterial communities of flooded paddy soil (Lüdemann, Arth and Liesack 2000) or the treatment of textile dyes (de Sousa *et al.* 2012). Recently, 16S rRNA gene surveys using high-throughput sequencing revealed diverse microbial communities within Winogradsky columns (Abbasian *et al.* 2015), which were structured over time (Esteban, Hysa and Bartow-McKenney 2015) or according to the sediment sources and depth (Rundell *et al.* 2014). Later studies suggest that the Winogradsky microbial community establishes by a founder effect followed by diversification and enrichment over time of specific or rare taxa. To our knowledge, Winogradsky columns have not been evaluated using both geochemical and microbial approaches after a long incubation period (>500 days) and in the context of sediment polluted by heavy metals.

Therefore, the purpose of this study was to explore the diversification of biogeochemical processes and microbial communities by depth and from the interior to the surface of the Winogradsky columns established with heavy-metal-polluted sediments. The zonation of biogeochemical processes was delineated after 520 days of incubation with chemical composition analyses of porewater and sediment samples, including sulphur stable-isotope analysis and the geochemical proportioning of Cu, Ni, Pb, Zn and Fe using sequential chemical extractions. In parallel, bacterial and archaeal 16S rRNA surveys were conducted to evaluate the diversity of microbial communities in the stratified habitats formed by geochemical gradients in the columns.

MATERIALS AND METHODS

Wetland sediments

Fifty kilograms of surface sediment (1–5 cm) was collected on 5 December 2012 from five zones of a shallow (<1 m depth) artificial stormwater wetland (Rouffach, Alsace, France; 47°57′9′ N, 7°17′3′ E). The wetland is situated at the outlet of a 42.7-ha vineyard catchment that collects stormwater and suspended solids that are mainly polluted by Cu and Zn (Babcsányi *et al.* 2014; Maillard and Imfeld 2014). The vegetation covered 80% of the wetland area, and *Phragmites australis* (Cav.) Steud. represented 90% of the total vegetation cover. The sediment was sieved (<2 mm) to remove large debris, thoroughly homogenised with a mixer and stored at 4°C until the columns were set up.

Column set-up

Duplicate glass columns were successively rinsed with 20% HCl, 18.2 MΩ cm water (Millipore, Billerica, MA, USA) and ethanol (96%). Relatively large glass columns (Ø: 15 cm, height: 65 cm) were used to collect large sediment samples (>240 cm³) and reduce the effect of heterogeneity when comparing samples. Planar oxygen sensor spots (Presens, Regenburg, Germany) were deployed in the inner part of the glass column at 15, 28, 38, 47 and 56 cm below the water surface for *in situ* measurement of dissolved oxygen. A PVC stand with a fixed perpendicular Teflon stick was placed at the bottom of the columns before packing the sediments to facilitate the extraction of an intact sediment core at the end of the experiment (see 'Sampling' section and Supplementary Fig. S1).

The physicochemical characteristics of the collected sediment are provided in Supplementary Table S1. The two columns were filled to 42 cm with sediment mixed to homogeneity with 4.5% (by weight) Na_2SO_4, 0.2% Na_2CO_3, 0.5% K_2HPO_4 and 0.5% NH_4SO_4 (Loss *et al.* 2013). Pure cellulose (0.7%) was added only to the bottom 19 cm of the column as a supplemental organic carbon source to establish a steep sulphide gradient within the column and favour fermentation. Air bubbles were removed using a spatula. The packed sediment was overlaid with a 19 cm layer of distilled water (3.4 L) at the top of the sediment column (42 cm of total sediment height). The columns were covered with a transparent Plexiglas disk secured with a rubber band to limit atmospheric contamination and water evaporation. The columns were incubated at 20°C with 12 h day^{-1} illumination using 150 W tungsten–halogen lamps for 520 days (74.3 weeks).

Sampling

The overlying water was collected after 520 days of incubation using plastic syringes and Teflon needles. For algal analysis, 100 mL of water was filtered at <12 μm and preserved by adding 0.25% (v:v) glutaraldehyde. For microbial DNA extraction, 250 mL of water was filtered through sterile 0.2 μm cellulose nitrate filters (Millipore, Billerica, MA, USA), which were then stored in sterile 50 mL Falcon tubes at −20°C until further processing. The top and bottom water layers (∼1.6 L each) of the overlying water were collected separately for hydrochemical analyses.

Intact sediment cores were extracted from the middle of each column by sinking a PVC tube (Ø: 12 cm, height: 65 cm) into the sediments up to the PVC support placed at the bottom of the column (Supplementary Fig. S1). The sediment core in the PVC tubes was then raised with the help of the Teflon stick

fixed to the PVC support placed in the columns before sediment packing (Supplementary Fig. S1). The intact cores were immediately frozen at $-20°$C. In addition, light-exposed sediment samples were collected along the column wall at 3, 8, 16 and 28 cm below the water–sediment interface (WSI) to evaluate changes in the microbial community in a latitudinal gradient from the light-exposed surface to the interior of the column (Supplementary Fig. S1). The frozen sediment cores collected in the middle of the columns were sliced into 2 cm layers (top 10 cm) and 6 cm layers (bottom section) with a tungsten saw, as steeper gradients were expected in the top 10 cm (Supplementary Fig. S1). Half of the layer was kept frozen until geochemical and sulphur isotope analyses. The other half-layers were thawed in a glove box (Jacomex BS531, Dagneux, France) under N_2 atmosphere ($<$1 ppm O_2). After homogenisation, 1 g of each layer was collected for DNA extraction and stored in sterile tubes at $-20°$C until further processing. The thawed sediment layers were centrifuged separately at 1700 *g* for 30 min (Jouan B4, Thermo Electron Corp., Waltham, MA, USA) to retrieve the porewater. Then, 2.5 mL of the porewater was filtered ($<$0.2 μm) using syringe filters under a nitrogen atmosphere for immediate Fe^{2+} analysis. The remaining porewater was filtered using 0.2 μm PTFE membranes, acidified with double-subboiled HNO_3 and stored at 4°C until hydrochemical analyses.

Analyses

Algae
Enumeration, taxonomic identification and biomass determination of algae in the overlying water (50:50 pooled sample from the top and bottom water layer sub-samples) was carried out at the GreenWater Laboratory (Palatka, FL, USA) following standard protocols (Hillebrand *et al.* 1999). Algal counts were carried out using an inverted microscope with phase contrast optics (Nikon Eclipse TE200, Tokyo, Japan).

Hydrochemistry
The pH, organic/inorganic carbon, alkalinity, conductivity, anions and major and trace elements of the filtrates were quantified using the FR EN ISO laboratory procedures, as described elsewhere (Lucas *et al.* 2010). Sulphide ions (S^{2-}) were quantified with Arrow probes (Lazar Research Laboratories, Inc., Los Angeles, CA, USA) under a N_2 atmosphere with an uncertainty of $\pm$0.5%. Ferrous iron (Fe^{2+}) was measured using a UV spectrophotometer (Shimadzu UV-1700, Pharmspec, Kyoto, Japan) with an uncertainty of $\pm$3%. Acetate was quantified by ion chromatography (ICS 3000 Dionex, San Diego, CA, USA) with an uncertainty of $\pm$2%.

Geochemistry
Sediment organic matter (OM) (SOL-0401), organic carbon (C_{org}) (NF ISO 10694), inorganic carbon (C_{inorg}) (NF ISO 10694), pH (in water) (NF ISO 10390), total carbon (C_{tot}) (NF ISO 10694), total nitrogen (N_{tot}) (NF ISO 13878), $N-NO_3^-$ and $N-NH_4^+$ (SOL-1402) were measured according to the NF ISO standards and procedures.

For chemical composition analysis, dried sediments were powdered using an agate disk mill ($<$63 μm) prior to alkaline fusion and total dissolution by acids, with measurements by inductively coupled plasma atomic emission spectroscopy (ICP-AES) and inductively coupled plasma mass spectrometry (ICP-MS) using the geological standards BCR-2 (US Geological Survey, Reston, VA, USA) and SCL-7003 (Analytika, Prague, Czech Republic) for quality control (Babcsányi *et al.* 2014). Fractionation

of Zn, Cu, Pb, Ni and Fe was quantified using a sequential extraction procedure adapted from previous methods (McKeague and Day 1966; Tessier, Campbel and Bisson 1979; Rauret *et al.* 2000) and detailed elsewhere (Semhi, Al Abri and Al Khanbashi 2014). Five fractions were sequentially extracted: (i) exchangeable (cation exchange), (ii) acid soluble (carbonate bound), (iii) reducible (Fe- and Mn-oxide bound), (iv) oxidisable (organic matter and sulphide bound) and (v) residual (silicate matrix and refractory sulphur species). Samples were treated under a N_2 atmosphere until the oxidisable stage to avoid oxidation of reduced sulphides. Special care was taken to avoid losing sediment material. Residues obtained at each extraction stage were washed for 5 min with 20 mL of 18.2 MΩ cm water (Millipore) using an end-over-end shaker and centrifuged (1700 *g*, 30 min). The residues recovered in the washing solutions were added to the previously extracted fraction. All solutions were acidified and stored at 4°C in polyethylene vials until analysis by ICP-AES and -MS. Based on separate triplicate extractions and measurements, the uncertainty of the fractionation data was $<$10% (Semhi, Al Abri and Al Khanbashi 2014).

Mineral phases in the initial sediment and selected sediment layers were identified by X-ray diffraction (XRD) analysis (Brüker D5000, Brüker Corp., Billerica, MA, USA) (3–65° 2θ scanning angle, 1 s–0.02° upwards step, Cu anticathode, wavelength λ Kα1 = 1.54056 Å, 30 mA 7, current: 30 mA, voltage: 40 kV).

S stable isotope analysis
Dried and powdered sediment samples were acidified with 1 M HCl, left overnight to remove inorganic carbon, neutralised by successively washing with distilled water and oven-dried at 60°C. The sulphur isotope composition was analysed using elemental analyser isotope ratio mass spectrometry (EA-IRMS) system. The furnace was held at 1080°C. Sediment samples plus a vanadium pentoxide catalyst were combusted in the presence of oxygen, and combusted gases were swept over combustion catalysts (tungstic oxide/zirconium oxide) and reduced with high-purity Cu wires. Sulphur dioxide was resolved from N_2 and CO_2 on a packed gas chromatography column at 32°C. For quality control, tin capsules of an IA-R061 in-house standard and the IAEA-SO-5 standard were regularly measured during the sequence. The analytical uncertainty that incorporates both accuracy and reproducibility for the mean δ^{34}S-values was $<$0.3‰. The δ^{34}S values (‰) were expressed relative to the Vienna Canyon Diablo Troilite (VCDT).

DNA extraction
Total DNA was extracted from the filters and the sediment with a PowerSoil® DNA Isolation Kit (MO BIO, Carlsbad, CA, USA) following the manufacturer's instructions. The concentrations of DNA were determined using a Qubit® fluorometer and Qubit® dsDNA HS Assay Kit (Invitrogen, Carlsbad, CA, USA).

Illumina MiSeq sequencing
Sequencing was performed at the Research and Testing Laboratory (Lubbock, TX, USA) using the Illumina MiSeq system (Illumina Inc. San Diego, CA, USA). The 16S rRNA gene spanning hypervariable region V4 was amplified in a two-step process. The study compared the concordance of results and overall performance of the primer sets 515F/806R (5′-GTGCCAGCMGCCGCGGTAA-3′/5′-GGACTACHVGGGTWTCTAAT-3′) (Walters *et al.* 2011), traditionally used by the Earth Microbiome Project (http://www.earthmicrobiome.org/emp-standard-protocols/16s/), and 519wF/909R (5′-CAGCMGCCGCGGTAA-3′/5′-TTTCAGYCTTGCGR

CCGTAC-3′) (Klindworth *et al.* 2013) for partial bacterial and archaeal 16S rRNA gene amplification.

The forward and reverse primers were constructed with the Illumina i5 (5′-TCGTCGGCAGCGTCAGATGTGTATAAGAGA CAG-3′) and the Illumina i7 (5′-GTCTCGTGGGCTCGGA GATGTGTATAAGAGACAG-3′) sequencing primers, respectively. Sequences were generated by PCR in 25 μL reactions with the Qiagen HotStar Taq master mix (Qiagen Inc, Valencia, CA, USA), and 1 μL of each 5 μM primer and 1 μL of template. Reactions were performed on ABI Veriti thermocyclers (Applied Biosytems, Carlsbad, CA, USA) under the following thermal profile: 95°C for 5 min, then 25 cycles of 94°C for 30 s, 54°C for 40 s, 72°C for 1 min, followed by one cycle of 72°C for 10 min and 4°C hold.

Products from the first stage amplification were added to a second PCR. Primers for the second PCR were designed based on the Illumina Nextera PCR primers as follows: forward, AATGATACGGCGACCACCGAGATCTACAC-[i5index]TCGTCGGCAGCGT and reverse, CAAGCAGAAGACG-GCATACGAGAT[i7index]GTCTCGTGGGCTCGG. The second stage amplification was run in the same conditions as in the first stage except for 10 cycles. Amplification products were visualised using eGels (Life Technology, Carlsbad, CA, USA). Products were pooled equimolar and each pool was size selected in two rounds using Agencourt AMPure XP (BeckmanCoulter, Indianapolis, IN, USA) in a 0.7 ratio for both rounds. Size selected pools were quantified using the Qubit 2.0 (Thermo Fisher Scientific, Inc., Waltham, MA, US) fluorometer (Life Technologies) and loaded at 10 pM on an Illumina MiSeq with 2 × 300 flow cells.

Data analysis

Processing of Illumina's MiSeq data
Denoising, chimera checking, generation of operational taxonomic units (OTUs) and taxonomic classification were performed using the custom-scripted bioinformatics pipeline of Research and Testing Laboratory (Lubbock, TX, USA). Briefly, denoising and generation of OTUs were accomplished after conversion into FASTA formatted sequences and quality files using USEARCH (Edgar 2010) and UPARSE OTU for OTU selection (Edgar 2013). Chimera checking was performed using UCHIME algorithms executed in *de novo* mode (Edgar *et al.* 2011). Sequences were clustered into OTUs at different levels of sequence identity using the UPARSE algorithm. The centroid sequence from each cluster was then run against the USEARCH global alignment algorithm against a highly curated database compiled by Research and Testing Laboratory and originating from NCBI (http://nbci.nlm.nih.gov). Based on the sequence identity percentage derived from BLASTn, sequences with identity scores to known or well-characterised 16S sequences >97% identity (<3% divergence) were resolved at the species level, >95 to 97% at the genus level, >90 to 95% at the family level, >80 to 90% at the order level, >80 to 85% at the class level and 77 to 80% at the phylum level. Any match below this level of identity was not used in taxonomic analysis. Matrices of taxonomic data were further used to visualise changes in community structures.

Microbial diversity and structure analysis
To visualise dissimilarities in bacterial and archaeal community structures, two-dimensional non-metric multidimensional scaling (NMDS) based on Bray–Curtis dissimilarities of Hellinger-transformed data (square-root transformation of relative abundances) was used. The relationship between the community profiles and biogeochemical variables was investigated by fitting environmental vectors *a posteriori* onto the NMDS, and their significance was assessed with a Monte-Carlo permutation test (1000 permutation steps).

To calculate the diversity and richness indices, the Illumina MiSeq sequences were down-analysed using MOTHUR version 1.36.1 (http://www.mothur.org) starting from denoised and chimera-checked sequences, aligned, and clustered to define OTUs at 97% sequence identity. A subsample of sequences was then randomly selected to obtain equally sized datasets according to the standard operating procedure (Schloss *et al.* 2009). The resulting datasets were used to calculate the diversity indices using R and for rarefaction analysis. Shannon's diversity index ($H′$) was calculated as $H' = -\sum p_i \ln p_i$, and the inverse Simpson's diversity index (S) was calculated as $S = 1/(1 - D)$ with $D = \sum p_{i2}$, where p_i is the relative abundance of species i. The Chao1 richness estimate was calculated as $S_{chao1} = S_{obs} + f_1^2/2f_2$, where S_{obs} is total number of OTUs in a sample, f_1 is the number of OTUs with only one sequence (i.e. 'singletons') and f_2 is the number of OTUs with only two sequences (i.e. 'doubletons').

RESULTS

Algal analysis

In overlying water, green algae (Chlorophyta) prevailed. In particular, the *Tetracystis* and *Chlorococcum* genera were present in unicellular and colonial forms, with a diameter ranging from 5.0 to 14.5 μm (Supplementary Fig. S2). The algal and volumetric biomass concentrations were larger in column 2 (232 × 10^3 cells mL^{-1}; 30 × 10^6 μm^3 mL^{-1}) than in column 1 (124 × 10^3 cells mL^{-1}; 13 × 10^6 μm^3 mL^{-1}). Lower algal concentrations in column 1 corresponded to a larger accumulation of dead algal matter at the WSI, as indicated by the higher concentrations of total and dissolved organic carbon, as well as total nitrogen (Fig. 1).

Biogeochemical gradients

The vertical profiles of the geochemical parameters for both porewater and sediments showed that the Winogradky columns had stratified after 520 days of incubation (Figs 1 and 2 and Supplementary Fig. S3). Globally, similar biogeochemical patterns were obtained for the duplicate columns. The abrupt increase in the average C:N ratios from ∼11 at the WSI to ∼25 down-core in the sediment (Fig. 1) can be attributed to a shift from mainly algal to vascular plant (i.e. *Phragmites australis*) dominance of organic carbon (Meyers and Ishiwatari 1993). Profiles of pH, inorganic and organic carbon, acetate and calcium showed carbonate dissolution with concomitant accumulation of organic-rich material and acetate production at the WSI (Fig. 1). In the zone beneath the WSI (23–29 cm below the water surface), depletion of organic matter (OM) and the increase of inorganic carbon (Fig. 1) suggest intense OM degradation. Dissolved O$_2$ was depleted in the first 10 cm below the WSI, while the NH$_4^+$, Fe^{2+}, S^{2-} and acetate concentrations increased down-core in the sediment, underscoring the gradients of terminal electron-accepting processes (TEAPs) (Figs 1 and 2).

The increase of alkalinity and S^{2-} with depth emphasised SO$_4^{2-}$ reduction. Both the increase in dissolved S^{2-} (up to 210 μM) below 50 cm (Fig. 2) and decrease in Fe^{2+} indicate the formation of FeS (black precipitates were observed in the columns, Supplementary Fig. S3). XRD analysis revealed the formation of pyrite in column 2 whereas pyrite could not be detected in the initial sediment (Supplementary Table S2).
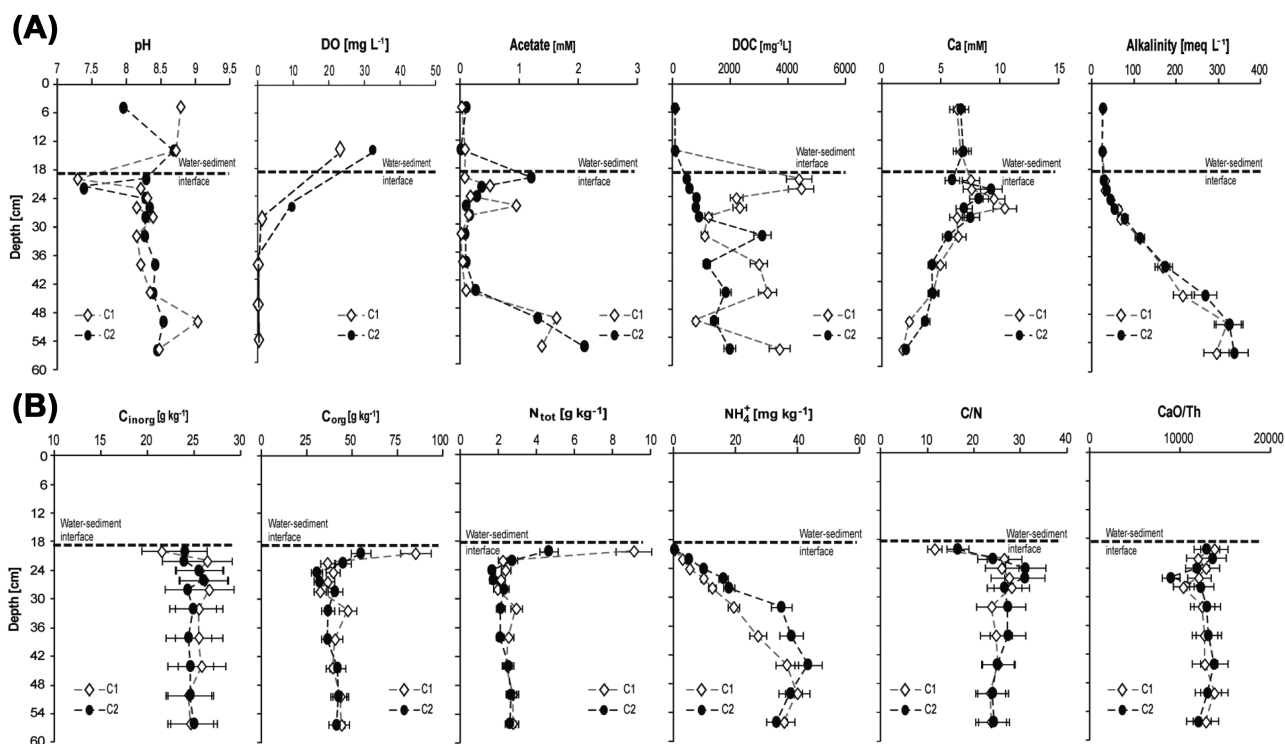
Figure 1. Vertical biogeochemical profiles in the overlying and porewater (**A**) and in the sediments (**B**) of the Winogradsky columns.
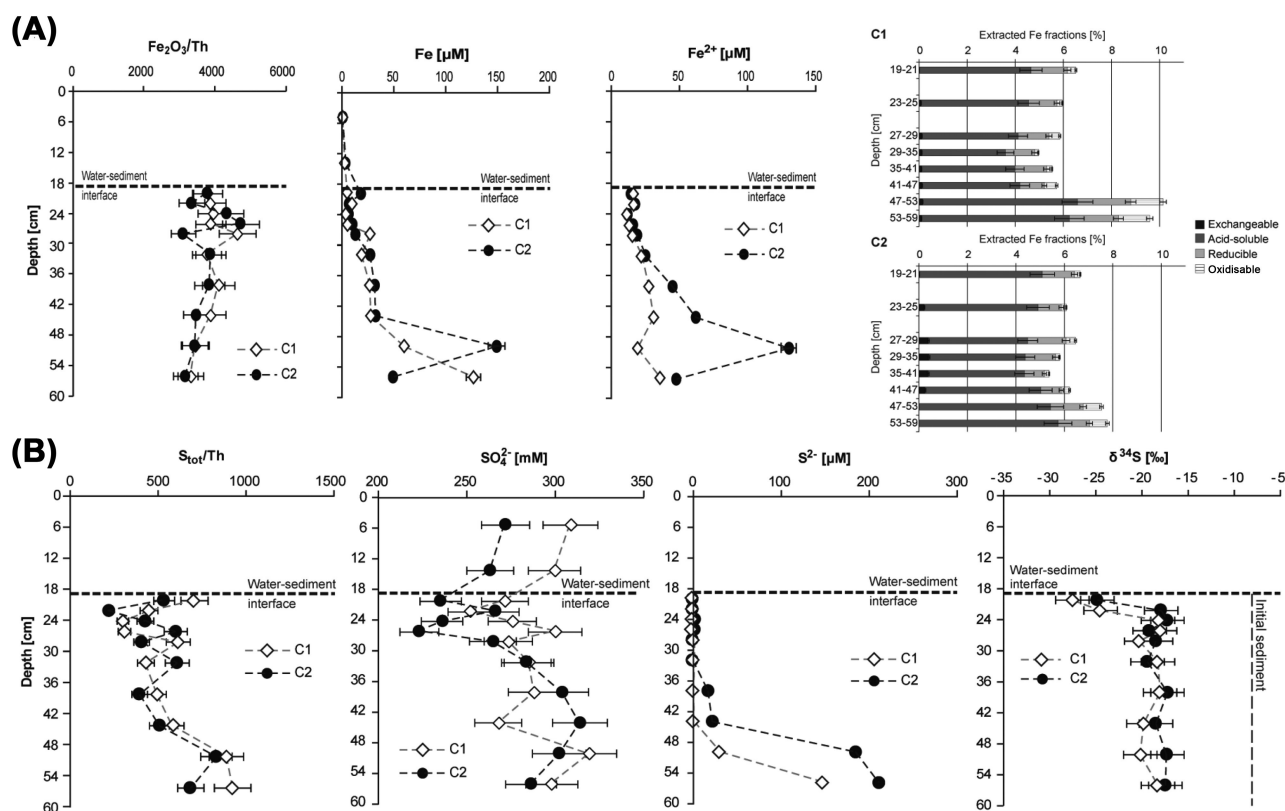

Figure 2. Iron (**A**) and sulphur (**B**) biogeochemistry in the Winogradsky columns 1 (C1) and 2 (C2). Changes in iron and total sulphur concentrations along the sediment profiles were evaluated accounting for dilution/concentration effects and are provided relative to thorium (Th) as a conservative element.
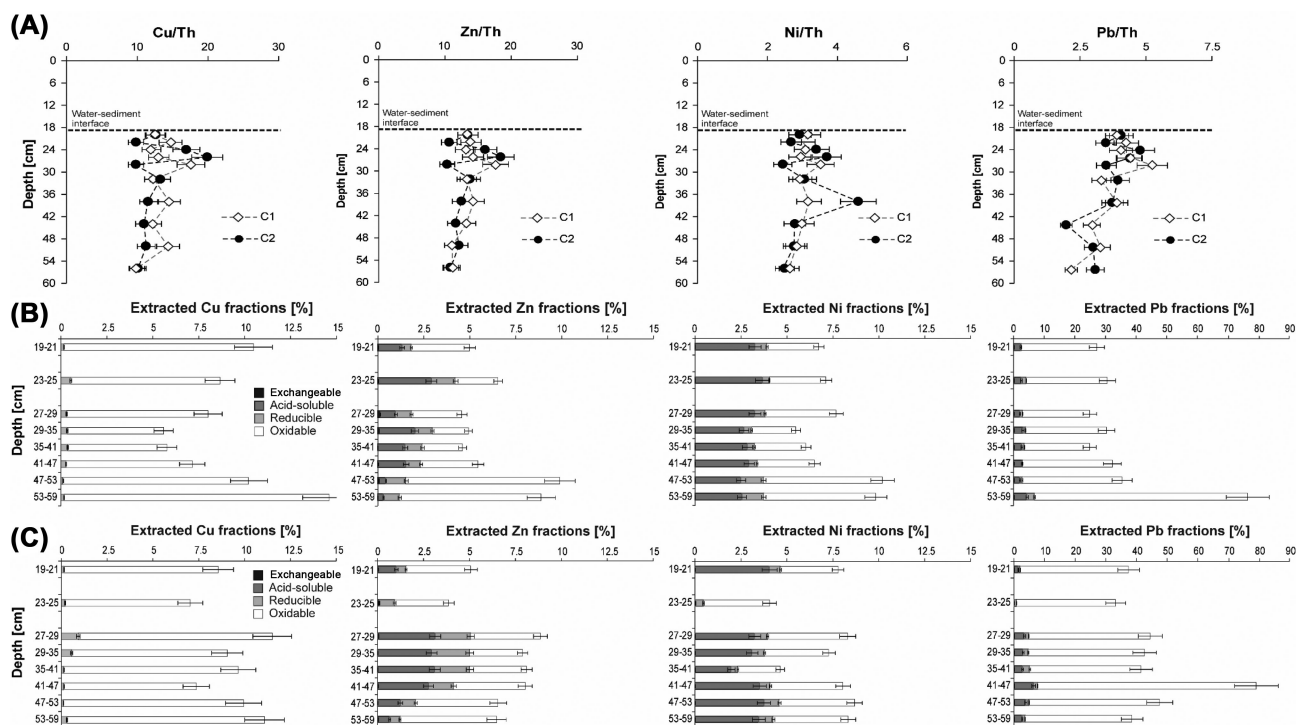
Figure 3. Vertical profiles of heavy metals in the sediment layers (relative to Th) (**A**) and relative proportions (% by weight) of non-residual fractions of Cu, Zn, Ni and Pb in column 1 (**B**) and column 2 (**C**). The residual fraction of heavy metals accounts for the remaining percentage (not displayed).

The abrupt change in the isotopic composition of sulphur (δ^{34}S) at the WSI also highlighted the stratification of SO_4^{2-} reduction in the columns (Fig. 2). The δ^{34}S values were constant below the WSI (-18.6 ± 1.0‰), which is consistent with active SO_4^{2-} reduction occurring in deeper anoxic zones. However, the δ^{34}S values abruptly decreased at the WSI (-25.7 ± 1.7‰), which suggests the oxidation to SO_4^{2-} of isotopically light S^{2-} diffusing upwards from the underlying zones of the columns.

Metal proportioning

While Cu, Zn and Pb concentrations in the sediment porewater were generally below the detection limit and low ($<40\ \mu$g L^{-1}), Ni concentrations gradually increased with depth up to 362 μg L^{-1} (Supplementary Table S3). The mean bulk sediment content ($\pm$SE) of Cu, Zn, Ni and Pb over depth was 121 ± 22, 131 ± 26, 30 ± 5 and $36 \pm 9\ \mu$g g^{-1}, respectively. Changes in heavy metal concentrations in the sediments are provided relative to thorium (Th) as a conservative element to account for dilution and concentration effects. The Th normalised concentrations emphasise slight enrichments in Fe, Cu and Zn ($+30$ to 60% compared with the initial sediment) from 4 to 10 cm below the WSI after 520 days of sediment incubation (Figs 2 and 3).

Different sequential extraction patterns for Cu, Zn, Ni and Fe reflected different sorption capacities of the metals on the wetland sediment. After 520 days of incubation, 85–95% of Cu, Zn, Ni and Fe was found in the residual fraction (silicate matrix and refractory sulphur species). In contrast, Pb (20–70% of total content) dominated in the oxidisable fraction (organic matter and sulphur-bound) below 40 cm (Figs 2 and 3). In addition to the residual fraction, Cu was also found in the oxidisable fraction (5–15%), while a minor proportion of Zn and Ni was associated with the acid-soluble and reducible fractions (2–5%). The non-residual fraction of Fe was mainly associated with the acid-soluble fraction and to a minor extent with the reducible fraction ($\leq$2%) (Fig. 2). Together with the minor proportion of Cu, Zn, Ni and Pb in the reducible fractions, this suggests that Fe(III) oxide-hydroxides influenced metal behaviour in the Winogradsky columns to a minor extent.

Diversity of microbial communities

A total of 834 283 (with 515F/806R primers, including 96.7% bacterial tags, 1.1% archaeal tags and 2.2% no-hits tags) and 796 426 (with 519wF/909R, including 95.3% bacterial, 2% archaeal and 2.6% no-hits tags) high-quality sequences ($>\sim$250 bp) were obtained from the 30 sediment samples. The mean number of tags per sample was 27 665 (515F/806R) and 26 218 (519wF/909R), respectively. The tags covered 27 phyla, 68 classes, 143 orders, 300 families and 488 genera. Although the sequencing depth did not systematically allow a survey of the full extent of microbial diversity (see Supplementary Fig. S4 for rarefaction curves), the patterns of beta diversity and the overall taxon relative abundances of the dominant lineages can be inferred (Bates *et al.* 2011). The rarefaction curves of diversity indices reached asymptotes (Supplementary Fig. S5), indicating that sampling was sufficient to capture the diversity of microbial communities.

The column communities were dominated by members of two main phyla (Proteobacteria and Firmicutes) that represent an average of 50% of each sample (515F/806R) (71% using 519wF/909R). Previous reports have also suggested that Proteobacteria are dominant in metal-contaminated sediments (Hemme *et al.* 2010; Gillan *et al.* 2015). Unknown Bacteria accounted for 2–43% (mean of 19%) of the total communities. More than 50% of genera composing the microbial communities in the Winogradsky columns had an abundance greater than 1% (excluding the contribution of unknown bacteria). This underscores that several abundant genera composed the communities. By
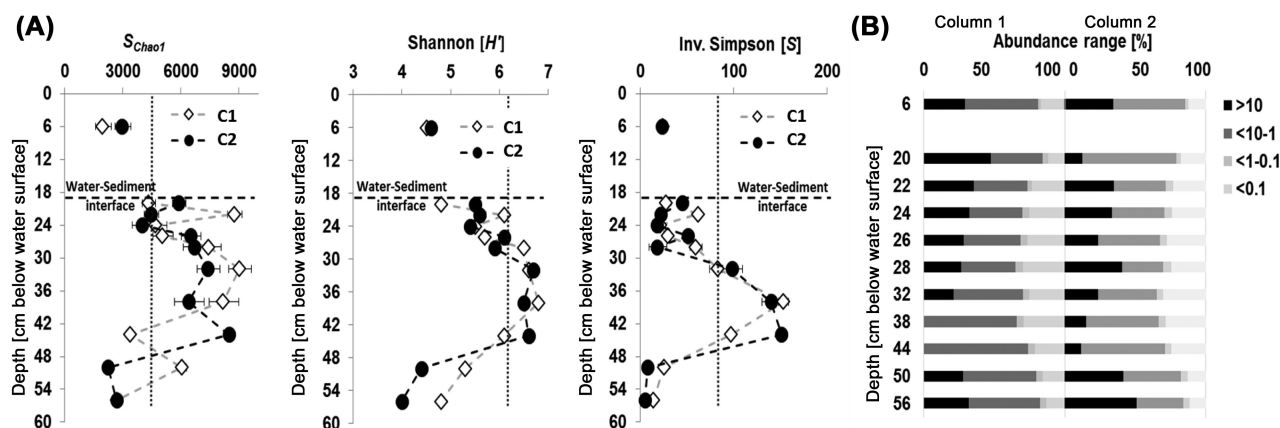
Figure 4. Richness, diversity and distribution of bacterial genera (OTUs at 97% sequence identity; using bacterial 515F/806R primers; 10 117 sequences sampled). (**A**) The error associated with the Chao 1, Shannon and Simpson indexes was <15%, <1.7% and <11% of the value, respectively, for column 1 (C1) and column 2 (C2). The vertical dashed lines indicate richness and diversity values of the initial sediment. (**B**) The relative distribution of abundant and rare genera is shown for columns 1 (left) and 2 (right).
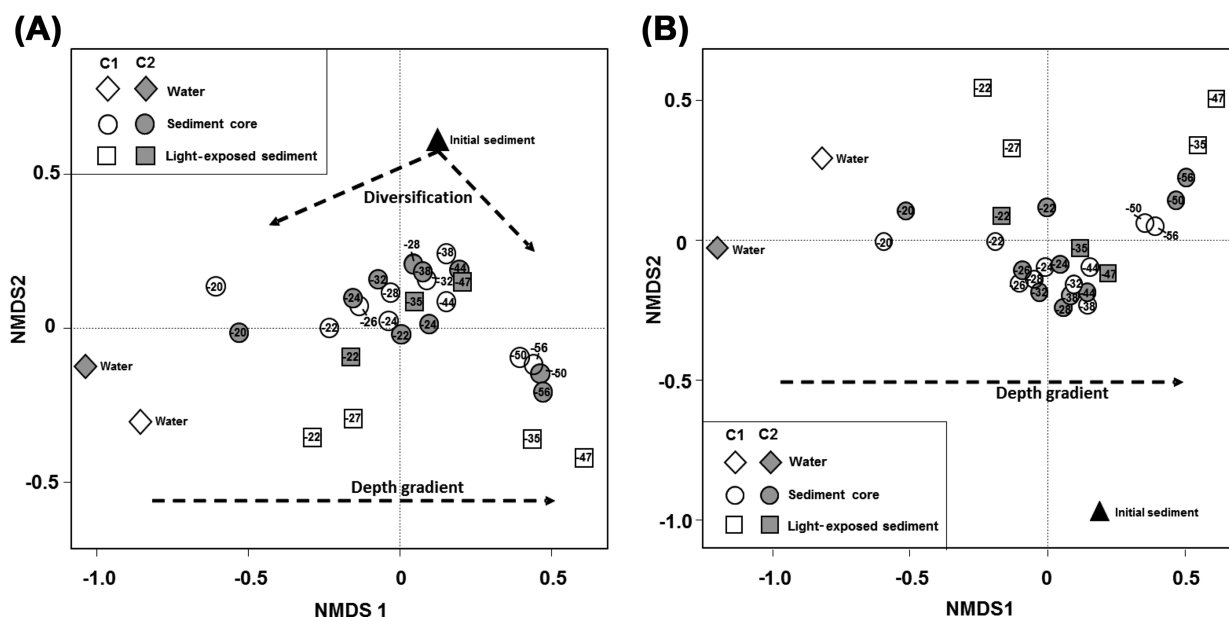

Figure 5. 2D-NMDS ordination of community profiles of Illumina MiSeq-sequenced samples of the Winogradsky columns obtained with (**A**) 515F/806R and (**B**) 519wF/909R primer pairs for column 1 (C1) and column 2 (C2). Numbers on the symbols indicate the depth (cm) below the water surface. Plot stress for (A) and (B): 0.08.

contrast, only approximately 20% of the genera were rare (<1% abundance) and 4% were very rare (<0.1% abundance) (Fig. 4 and Supplementary Fig. S6).

In terms of the metrics of microbial diversity, Shannon and inverse Simpson diversity, unlike the S_{chao1} abundance-based richness estimator, differed significantly with depth (Fig. 4 and Supplementary Fig. S6). Compared with the initial sediment, microbial diversity in both columns was higher in samples of the middle of the sediment profile (depth: 30–48 cm) and lower in samples from the WSI and bottom zone (below 48 cm).

Diversification and composition of microbial communities

Changes in microbial assemblages were visualised by the NMDS ordination of Illumina MiSeq data (Fig. 5.). The microbial community of the initial sediment clearly differed from

all other samples, which emphasises niche differentiation from the founding populations to clearly distinct communities. Column sediment samples were mainly discriminated according to depth. Water and WSI samples differed from sediment samples (P = 0.01). Similar patterns were observed for the two columns, and the datasets obtained with the 515F/806R and 519wF/909R primer pairs yielded concordant results and overall performance.

The Winogradsky columns were characterised by major differences in the abundance of bacterial and archaeal taxonomic groups with depth and from the surface to interior of the columns (Supplementary Figs S7 and S8). Proteobacteria, which are often linked to the oxic zones of redox gradients (Brune, Frenzel and Cypionka 2000), were specifically abundant in the overlying water layer and the first sediment layers. In contrast, Firmicutes and class Bacteroida dominated down-core, below 30 cm depth (or 12 cm below the WSI). Changes in the microbial community composition are discussed below in relation to

the diversification of biogeochemical processes observed along the Winograsky columns, including changes in nutrients, redox-sensitive species and metal proportioning.

DISCUSSION

In this study, high-throughput sequencing was complemented by elemental and metal proportioning analyses to evaluate the relationship between chemical conditions and microbial communities along biogeochemical gradients stabilised for 520 days in Winogradsky columns. To evaluate this relationship, the biogeochemical parameters (i.e. nutrients, carbon, metals, ions, metal fractions) were fitted *a posteriori* onto the NMDS ordination of community profiles from the core sediment samples (Supplementary Fig. S9). The NMDS ordination revealed that the microbial community composition correlated best with changes in S^{2-}, NH_4^+, Na^+, K^+, acetate, PO_4^{3-}, HCO_3^-, alkalinity ($P < 0.001$), and to a minor extent with changes in NO_3^-, Ca^{2+}, Mg^{2+}, CO_3^{2-}, total iron and Ni in porewater ($P < 0.01$). This result is in agreement with the composition of microbial assemblages that were not specific to polluted environments, but rather reflected nutrient and redox gradients as well as geochemical zonation.

Elemental and nutrient gradients in the Winogradsky column mainly resulted from the differentiation of microbial niches as well as the algal nutrient uptake. For instance, decreasing Na^+ and K^+ concentrations from the bottom to the top of the column and slightly higher concentrations in the water layer (Supplementary Table S3) indicated nutrient diffusion from the sediment to the water. The assimilation of PO_4^{3-} and NH_4^+ by algal cells in the water and CO_2 consumption during photosynthesis determined the concentration profiles of these nutrients in the porewater beneath the WSI. In the overlying water layer, Proteobacteria populations were dominated by the class Alphaproteobacteria, and genera such as *Parvibaculum* and *Tistlia*, known to develop under aerobic conditions. Although algal colonisation along the column wall was associated with oxygen production (Fig. 1), oxygen was probably depleted radially towards the interior of the sediment layers due to oxygen consumption by aerobic heterotrophic microorganisms. These include Betaproteobacteria, which were particularly abundant at the WSI. Similarly, microbial oxygen consumption with depth is expected to exceed diffusive oxygen supply from algae in the overlying water, and thus favour the use of alternative terminal electron acceptors, such as Fe^{3+} and sulphate.

Carbon cycling in Winogradsky columns is mainly controlled by the mineralisation of sediment organic matter (OM) and CO_2 incorporation into the biomass of autotrophic microorganisms. The intense OM mineralisation observed in the zone immediately below the WSI (i.e. 24–30 cm depth; Fig. 1) can be related to the broad diversity of organic carbon sources derived from both sediment and algae. In addition, lower concentrations of toxic H_2S in the zone immediately below the WSI, compared with H_2S concentrations at the bottom of the columns, may have impacted above communities to a lesser extent. Higher acetate concentrations at and below the WSI (Fig. 1) suggest a lower consumption rate of acetate by Fe^{3+}- and/or sulphate-reducing microorganisms due to the occurrence of more favourable terminal electron acceptors, such as oxygen and nitrate. Carbonate dissolution in sediments may theoretically be attributed to pH decrease induced by pyrite oxidation and/or CO_2 production during heterotrophic breakdown of OM and algal respiration (du Laing *et al*. 2009; Cirkel *et al*. 2014). However, pH was buffered in our case and molar ratios of ~0.3 to ~0.4 of Ca+Mg over HCO_3^-

(Supplementary Table S3) could be observed. This supports the idea that CO_2 production mainly caused carbonate dissolution at the WSI and the zone below the WSI (i.e. 24–30 cm depth; Fig. 1).

Interestingly, OM mineralisation and carbonate dissolution at and below the WSI was associated with relatively low microbial diversity and richness and a microbial composition differing from that of the overlying water and the bottom sediments. This may be due to the selection pressure exerted by prevailing algal-derived carbon sources with a low C:N ratio. Similarly, supplemental cellulose (0.7% w:w) in the bottom layers (<19 cm) likely reduced diversity while favouring fermentative processes (Rundell *et al*. 2014). Overall, the low relative proportion of rare (<20%) and very rare (<4%) taxa found in the Winogradsky columns after 520 days of incubation contrasts with previous results showing that 61–78% of genera were very rare after 126 days of incubation (Rundell *et al*. 2014). This suggests that longer incubation periods can enhance drastic changes in both nutrients and accumulation of metabolic products, and favour the dominance of slow growing microorganisms over time while apparently reducing rare genera. However, in our case, the degree of precision with which the community was examined may not be sufficient to strictly confirm the occurrence or disappearance of specific phylotypes. Changes in the chemical reactions in the columns through the development of depth-specific microbial metabolism can also gradually increase the abundance of more slowly growing organisms while decreasing that of initially active ones found in the freshly collected sediments. For instance, Cyanobacteria remained abundant only in the light-exposed zones (WSI and light-exposed sediment) compared with the initial sediment (Supplementary Fig. S7). Cyanobacteria (>12%) but also Betaproteobacteria (>35%) (order Rhizobiales) mostly appeared in the WSI layers, as well as Chloroflexi of the non-phototropic class Anaerolinea and free-floating filamentous cyanobacteria of the *Arthrospira* genus and Alphaprotebacteria, including the strictly aerobic genus *Phenylobacterium*. Overall, Betaproteobacteria increased in the WSI while Firmicutes increased by one order of magnitude at the bottom of the columns after 520 days of incubation. In the lower depths, Firmicutes (Clostridia, genera *Clostridiisalibacter* and *Candidatus*), but also Bacteroidetes (order Bacteroidales and Cytophagales) and the ammonia-oxidising *Thaumarchaeota* (genus *Nitrososphaera*) generally increased in abundance with depth.

The iron cycle in the Winogradsky columns was mainly evidenced by microbial Fe^{3+} reduction with local Fe mobilisation (see the Th normalised depth profile of sediment-bound Fe, Fig. 2), and pyrite oxidation at the WSI. In addition, pyritisation following Fe^{3+} reduction was evidenced by XRD analysis (Supplementary Table S2). Increase of total and ferrous iron concentrations as well as acetate in the porewater of the bottom sediments (i.e. below 48 cm) indicates that microbial Fe reduction contributed to the diagenesis of organic matter. Fe enrichment between 4 and 10 cm below the WSI (Fig. 2) coincided with higher OM mineralisation. Pyrite reoxidation at the WSI as well as Fe mobilisation from the bottom sediment layers (Fig. 2) during dissimilatory Fe^{3+} reduction (Lovley, Holmes and Nevin 2004) can both contribute to Fe redistribution with depth. Iron reducing microorganisms in sediments are phylogenetically diverse. Proteobacteria and Firmicutes, which were particularly abundant down-core below the WSI, are typically the dominant groups among the iron-reducing communities in sediments (e.g. Li *et al*. 2011). However, the presence in the light-exposed sediment below the WSI of *Thiocapsa,* which can oxidise sulphides that diffuse upwards from underlying zones to the WSI, supports

the idea that pyrite oxidation occurred at the WSI. This is also in agreement with the sulphur stable isotope analysis.

The trend in S isotopic composition reflects a mostly closed reaction system with continued SO_4^{2-} reduction. The remaining SO_4^{2-} and S^{2-} in the sedimentary porewater became progressively enriched in ^{34}S when the rate of SO_4^{2-} reduction and precipitation of FeS exceeded that of diffusion (Canfield, Raiswell and Botrell 1992; Ryu *et al.* 2006). However, gypsum precipitation may also have contributed to the consumption of dissolved sulphate because the porewater was saturated with regards to gypsum (solubility product constant for gypsum, $K_{sp} = 2.5 \times 10^{-5}$). Based on the sulphate mass balance after 520 days of incubation, sulphate consumption rates were estimated to range from 0.30 μmol SO_4^{2-} cm^{-3} day^{-1} in the WSI zone up to 0.49 μmol SO_4^{2-} cm^{-3} day^{-1} at the bottom of the columns. Although such high rates are rarely found in natural lake sediments, they are similar to those observed in sulphate-rich lake sediments (0.30 μmol SO_4^{2-} cm^{-3} day^{-1}) or in seawater sediments (Habicht and Canfield 1997; Holmer and Storkholm 2001). These results are in agreement with the occurrence of several strictly anaerobic sulfate-reducing bacteria along the Winogradsky columns, including genera such as *Desulfatitalea*, *Desulfosarcina*, *Desulfobulbus*, *Desulfocapsa*, *Desulfofustis*, *Desulfofaba* and *Desulfococcus* of the Desulfobacteraceae family (Proteobacteria).

Overall, changes in microbial communities were mainly associated with nutrients as well as oxidation and reduction of iron and sulphur rather than with heavy metal proportioning. Despite the known limitations of the sequential extraction procedures (Tessier, Campbel and Bisson 1979; Rauret *et al.* 2000), proportioning of heavy metals in sediments allows evaluation of the influence of organo-mineral phases on their availability and mobility in sediments. However, it does not provide direct information about their toxicity in multi-polluted sediments (Baran and Tarnawski 2015), which may be obtained by probing the microbial response (Imfeld and Vuilleumier 2012). After 520 days of incubation, the potentially mobile fraction of heavy metals in the Winogradsky column (i.e. including the carbonate-bound, Fe/Mn oxides and organic matter-bound fractions) was low in all sediment strata ($\leq$12%) (Fig. 3). Release of heavy metals and response of microbial communities are thus expected to be limited unless dramatic changes (e.g. pH or redox) in the physicochemical conditions of the sediment occur with time or column depth. Nevertheless, the correlation analysis suggests that changes in microbial communities may be associated with porewater concentrations of Ni that increased with the column depth. While nickel homeostasis has been recognised as a general microbiological concern, to date, the mechanisms of nickel toxicity in microorganisms remain poorly understood (Macomber and Hausinger 2011).

Metals associated with the residual fraction in sediments increased over the 520 days of incubation owing to their migration to higher energy binding sites (Ma *et al.* 2006; Du Laing *et al.* 2009). For instance, more than 50% of Cu in the initial sediment was in the acid-soluble (carbonate-bound), reducible (Fe- and Mn-oxide bound) and oxidisable fractions (Supplementary Fig. S10), whereas Cu was mainly associated with the residual fraction after 520 days of incubation (Fig. 3). Change of Cu proportioning over time (Supplementary Fig. S10) suggests that microbial communities responded to heavy metals in the early stage of the incubation, but diversified according to the zonation of biogeochemical activities in the latter incubation stages.

The slight enrichments in Cu, Zn, Ni and Pb in the zone from 4–10 cm below the WSI indicate metal migration between sediment layers during the 520 days of incubation (Fig. 3). In anoxic sediments, the Cu, Zn, Ni and Pb concentrations can be affected by the degradation of OM and carbonate dissolution, with the concomitant release of sediment-bound metals, the formation/dissolution of Fe(III) and Al oxide-hydroxide or redox-induced changes of sulphur forms and subsequent sequestration/mobilisation of reduced metal sulphides (Du Laing *et al.* 2009). Both OM degradation and calcite dissolution occurred below the WSI as well as the partial reoxidation of metal sulphides at the WSI likely contributed to the depth down-distribution of Cu, Ni, Zn and Pb. In addition, Fe enrichment below the WSI and change in Cu proportioning during sediment aging suggest the release of calcite- and OM-bound metals with concomitant formation of more refractory metal sulphide phases, such as pyrite (included in the residual fraction). In the bottom of the columns, the formation of soluble bisulphide and polysulphide complexes with Cu, Ni and Zn at high sulphide concentrations (<30 μmol L^{-1}) (Huerta-Diaz, Tessier and Carignan 1998) likely increased metal concentrations in porewater.

CONCLUSION

This study delineated the spatial distribution of bacteria with depth and from light-exposed surfaces to the interior of the sediment cores using Winogradsky columns established with metal-polluted sediments incubated during 520 days. It is postulated that niche differentiation occurred mainly by depth in the mature columns, while diversification was driven by biogeochemical gradients and depth-specific carbon sources at the WSI and the bottom of the columns. Such reproducible differentiation processes in Winogradsky columns can help in understanding how a diverse microbial community develops over time and adapts to biogeochemical fluctuations in polluted sediments. Changes in the chemical composition of the initial sediments along biogeochemical gradients in the Winogradsky columns highlight the role of microorganisms and related TEAPs in the cycling of iron, sulphur and heavy metals. One significant finding is that the distribution of microorganisms with depth was mainly associated with potential niches of prevailing TEAPs rather than heavy-metal distribution in the sediments. As expected, a very large proportion of heavy metals was immobilised in the residual fraction, thereby limiting the community response induced by toxic metals, with the exception of Ni in porewater. If physicochemical conditions change with time or depth, metals may be progressively released. Winogradsky column may thus serve to evaluate risks of heavy-metal mobilisation and release and its potential impact on organisms when biogeochemical conditions vary in dynamic environments. In particular, delineating the distribution of microbial communities and pollutant mobility at steep gradients at the WSI and over time may be crucial in the future for predicting functioning of the WSI in polluted aquatic ecosystems.

SUPPLEMENTARY DATA

Supplementary data are available at FEMSEC online.

ACKNOWLEDGEMENTS

REFERENCES

Abbasian F, Lockington R, Mallavarapu M *et al*. A pyrosequencing-based analysis of microbial diversity governed by ecological conditions in the Winogradsky column. *World J Microbiol Biotechnol* 2015;**31**:1115–26.

Babcsányi I, Imfeld G, Granet M *et al*. Copper stable isotopes to trace copper behavior in wetland systems. *Environ Sci Technol* 2014;**48**:5520–9.

Baran A, Tarnawski M. Assessment of heavy metals mobility and toxicity in contaminated sediments by sequential extraction and a battery of bioassays. *Ecotoxicology* 2015;**24**:1279–93.

Bates S, Berg-Lyons D, Caporaso J *et al*. Examining the global distribution of dominant archaeal populations in soil. *ISME J* 2011;**5**:908–17.

Borch T, Kretzschmar R, Kappler A *et al*. Biogeochemical redox processes and their impact on contaminant dynamics. *Environ Sci Technol* 2010;**44**:15–23.

Brune A, Frenzel P, Cypionka H. Life at the oxic-anoxic interface: microbial activities and adaptations. *FEMS Microbiol Rev* 2000;**24**:691–710.

Canfield D, Raiswell R, Botrell S. The reactivity of sedimentary iron mineral towards sulfide. *Am J Sci* 1992;**292**:659–83.

Cirkel D, Van Beek C, Witte J *et al*. Sulphate reduction and calcite precipitation in relation to internal eutrophication of groundwater fed alkaline fens. *Biogeochemistry* 2014;**117**:375–93.

de Sousa M, de Moraes P, Lopes P *et al*. Textile dye treated photo-electrolytically and monitored by winogradsky columns. *Environ Eng Sci* 2012;**29**:180–5.

Du Laing G, Rinklebe J, Vandecasteele B *et al*. Trace metal behaviour in estuarine and riverine floodplain soils and sediments: A review. *Sci Total Environ* 2009;**407**:3972–85.

Dworkin M. Sergei Winogradsky: a founder of modern microbiology and the first microbial ecologist. *FEMS Microbiol Rev* 2012;**36**:364–79.

Edgar R. Search and clustering orders of magnitude faster than BLAST. *Bioinformatics* 2010;**26**:2460–1.

Edgar R. UPARSE: highly accurate OTU sequences from microbial amplicon reads. *Nat Methods* 2013;**10**:996–8.

Edgar R, Haas B, Clemente J *et al*. UCHIME improves sensitivity and speed of chimera detection. *Bioinformatics* 2011;**27**:2194–200.

Esteban D, Hysa B, Bartow-McKenney C. Temporal and spatial distribution of the microbial community of Winogradsky columns. *PloS One* 2015;**10**:e0134588.

Gillan D, Roosa S, Kunath B *et al*. The long-term adaptation of bacterial communities in metal-contaminated sediments: a metaproteogenomic study. *Environ Microbiol* 2015;**17**:1991–2005.

Gounou C, Bousserrhine N, Varrault G *et al*. Influence of the iron-reducing bacteria on the release of heavy metals in anaerobic river sediment. *Water Air Soil Pollut* 2010;**212**:123–39.

Habicht KS, Canfield DE. Sulfur isotope fractionation during bacterial sulphate reduction in organic-rich sediments. *Geochim Cosmochim Acta* 1997;**61**:5351–61.

Hemme C, Deng Y, Gentry T *et al*. Metagenomic insights into evolution of a heavy metal-contaminated groundwater microbial community. *ISME J* 2010;**4**:660–72.

Hillebrand H, Dürselen C-D, Kirschtel D *et al*. Biovolume calculation for pelagic and benthic microalgae. *J Phycol* 1999;**35**:403–24.

Holmer M, Storkholm P. Sulphate reduction and sulphur cycling in lake sediments. *Freshw Biol* 2001;**46**:431–51.

Huerta-Diaz MA, Tessier A, Carignan R. Geochemistry of trace metals associated with reduced sulphur in freshwater sediments. *Appl Geochem* 1998;**13**:213–33.

Imfeld G, Vuilleumier S. Measuring the effects of pesticides on bacterial communities in soil: A critical review. *Eur J of Soil Biol* 2012;**49**:22–30.

Klindworth A, Pruesse E, Schweer T *et al*. Evaluation of general 16S ribosomal RNA gene PCR primers for classical and next-generation sequencing-based diversity studies. *Nucleic Acids Res* 2013;**41**:e1.

Li H, Peng J, Weber KA *et al*. Phylogenetic diversity of Fe(III)-reducing microorganisms in rice paddy soil: enrichment cultures with different short-chain fatty acids as electron donors. *J Soils Sediments* 2011;**11**:1234–42.

Loss R, Fontes M, Reginatto V *et al*. Biohydrogen production by a mixed photoheterotrophic culture obtained from a Winogradsky column prepared from the sediment of a southern Brazilian lagoon. *Renew Energy* 2013;**50**:648–54.

Lovley DR, Holmes DE, Nevin KP. Dissimilatory Fe(III) and Mn(IV) reduction. *Microb Rev* 2004;**49**:219–86.

Lucas Y, Schmitt AD, Chabaux F *et al*. Geochemical tracing and hydrogeochemical modelling of water–rock interactions during salinization of alluvial groundwater (Upper Rhine Valley, France). *Appl Geochem* 2010;**25**:1644–63.

Lüdemann H, Arth I, Liesack W. Spatial changes in the bacterial community structure along a vertical oxygen gradient in flooded paddy soil cores. *Appl Environ Microbiol* 2000;**66**:754–62.

Ma Y, Lombi E, Oliver I *et al*. Long-term aging of copper added to soils. *Environ Sci Technol* 2006;**40**:6310–7.

Machado A, Spencer K, Kloas W *et al*. Metal fate and effects in estuaries: A review and conceptual model for better understanding of toxicity. *Sci Total Environ* 2016;**541**:268–81.

Macomber L, Hausinger RP. Mechanisms of nickel toxicity in microorganisms. *Metallomics* 2011;**3**:1153–62.

Maillard E, Imfeld G. Pesticide mass budget in a stormwater wetland. *Environ Sci Technol* 2014;**48**:8603–11.

Martinez-Alonso M, Mir J, Gaju N *et al*. Morphological and ultrastructural characterization of an unusual purple sulfur bacterium from a marine microbial-mat community. *Micron* 2006;**37**:538–43.

McKeague JA, Day JH. Dithionite- and oxalate-extractable Fe and Al as aids in differentiating various classes of soils. *Can J Soil Sci* 1966;**46**:13–22.

Meyers P, Ishiwatari R. Lacustrine organic geochemistry – an overview of indicators of organic-matter sources and diagenesis in lake-sediment. *Org Geochem* 1993;**20**:867–900.

Morse J, Luther G. Chemical influences on trace metal-sulfide interactions in anoxic sediments. *Geochim Cosmochim Acta* 1999;**63**:3373–8.

Pedersen L, Smets B, Dechesne A. Measuring biogeochemical heterogeneity at the micro scale in soils and sediments. *Soil Biol Biochem* 2015;**90**:122–38.

Rauret G, Lopez-Sanchez J, Sahuquillo A *et al*. Application of a modified BCR sequential extraction (three-step) procedure for the determination of extractable trace metal contents in a sewage sludge amended soil reference material (CRM 483), complemented by a three-year stability study of acetic acid and EDTA extractable metal content. *J Environ Monit* 2000;**2**:228–33.

Rundell E, Banta L, Ward D *et al.* 16S rRNA gene survey of microbial communities in Winogradsky columns. *PloS One* 2014;**9**:e104134.

Ryu J, Zierenberg R, Dahgren R *et al.* Sulfur biogeochemistry and isotopic fractionation in shallow groundwater and sediments of Owens Dry Lake, California. *Chemi Geol* 2006;**229**: 257–72.

Schloss P, Westcott S, Ryabin T *et al.* Introducing mothur: open-source, platform-independent, community-supported software for describing and comparing microbial communities. *Appl Environ Microbiol* 2009;**75**:7537–41.

Semhi K, Al Abri R, Al Khanbashi S. Impact of sewage and mining activities on distribution of heavy metals in the water-soil-vegetation system. *Int J Environ Sci Technol* 2014;**11**:1285–96.

Simpson S, Ward D, Strom D *et al.* Oxidation of acid-volatile sulfide in surface sediments increases the release and toxicity of copper to the benthic amphipod *Melita plumulosa*. *Chemosphere* 2012;**88**:953–61.

Tessier A, Campbel P, Bisson M. Sequential extraction procedure for the speciation of particulate trace-metals. *Analyt Chem* 1979;**51**:844–51.

Van der Gucht K, Cottenie K, Muylaert K *et al.* The power of species sorting: Local factors drive bacterial community composition over a wide range of spatial scales. *Proc Natl Acad Sci U S A* 2007;**104**:20404–9.

Walters W, Caporaso J, Lauber C *et al.* PrimerProspector: de novo design and taxonomic analysis of barcoded polymerase chain reaction primers. *Bioinformatics* 2011;**27**:1159–61.

Weber FA, Voegelin A, Kaegi R *et al.* Contaminant mobilization by metallic copper and metal sulphide colloids in flooded soil. *Nat Geosci* 2009;**2**:267–71.

Winogradski S. *Beiträge zur Morphologie und Physiologie der Bacterien. Heft I. Zur Morphologie und Physiologie der Schwefelbacterien*. Leipzig: Arthur Felix, 1888.